ACS MATERIALS LETTERS

www.acsmaterialsletters.org

LETTER

Engineering Caged Microbubbles for Controlled Acoustic Cavitation and Pressure Sensing

Yifeng Peng,*,¶ Chenguang Peng,¶ Tien Nguyen, Tao Sun, Tyrone Porter, Nathan McDannold, John N. Kheir, and Brian D. Polizzotti*

Cite This: *ACS Materials Lett.* 2021, 3, 978–987

Read Online

ACCESS | Metrics & More | Article Recommendations | Supporting Information

ABSTRACT: **Acoustic microbubbles (MBs) are an important class of biomaterials that play an increasingly prominent role in advanced applications such as contrast and super-resolution imaging, sonoporation, drug delivery, microrobotics, and biosensors. The ability to control and regulate acoustic cavitation of MBs by ultrasound (US) pulses is fundamental to achieve these applications. However, most MBs are coated with a soft shell that may undergo alteration (e.g., rupture or dissolution) under insonification and result in unintended acoustic responses. This work introduces a system of stable polymeric caged MBs in which the gas core is encapsulated within a rigid but nanoporous shell, so that their acoustic response is regulated by both shell compressibility and metastructure (i.e., porosity), thus permitting high control over their cavitation behaviors via pulse manipulation. These caged MBs are fabricated via a method of interfacial nanoprecipitation. Fabrication parameters can be varied to manipulate shell elasticity and porosity and subsequently control a wide range of acoustic properties such as tuning resonance frequency, controlling modes of nonlinear cavitation. Furthermore, the cavitation of caged MBs can be manipulated to develop tunable acoustic pressure sensors. These caged MBs offer insight of the acoustic−material relationship to design acoustic biomaterials for US-guided diagnostic and therapeutic technologies.**

Acoustic microbubbles (MBs) have emerged as a unique type of biomaterial because they undergo notable volumetric oscillations when exposed to ultrasound (US), that is, acoustic cavitation.[1] This phenomenon serves as the basis for the development of contrast-enhanced US imaging technologies, as the oscillating MBs emit strong echo signals in body that are distinct from tissue.[2] Furthermore, the use of acoustic MBs provides a unique tool to manipulate biological systems, as focused ultrasonic waves produce mechanical forces and/or heat at the tissue and cellular level; for example, an oscillating MB near a cell may generate streaming in the liquid that disrupts the cell membrane.[3] Hence, the application of acoustic MBs has become increasingly popular for fields beyond the improvement of contrast in standard imaging, including drug delivery,[4] tumor ablation,[5] super resolution imaging,[6] hemodynamic monitoring,[7] sonothrombolysis,[8] and microrobotics,[9] among others.[1−3] Central to the success of these applications, is the ability to generate desirable modes and amplitudes of MB cavitation. In general, the cavitation response of a pure gas bubble can be divided into the following three groups depending on how much energy is transferred from US pulses (in the order of low to high): [1] linear stable cavitation: MBs oscillate in very small amplitude with symmetrical change in shape, exerting minimal disturbance on the surrounding; [2] nonlinear stable cavitation: MBs oscillate in moderate to high amplitude with asymmetrical changes in shape, resulting in production of harmonic signals, exerting moderate mechanical influence on the surrounding—this type of cavitation is most preferrable for contrast imaging and drug delivery; [3] inertial cavitation: MBs undergo violent collapse, producing high mechanical energy and heat—this mode of action is desirable for targeted tumor ablations and for certain advanced imaging applications (e.g., blood flow); however, care must be taken as its use can cause harmful side-effects (e.g., damaged vasculature causing hemorrhage). However, because MBs must be stabilized by a coating material that consequently alter and complicate their acoustic response,[10] pulse

Received: May 17, 2021
Accepted: June 4, 2021
Published: June 7, 2021

Downloaded via NORTHEASTERN UNIV on March 4, 2026 at 15:34:46 (UTC).
See https://pubs.acs.org/sharingguidelines for options on how to legitimately share published articles.

© 2021 American Chemical Society

https://doi.org/10.1021/acsmaterialslett.1c00296
ACS Materials Lett. 2021, 3, 978–987

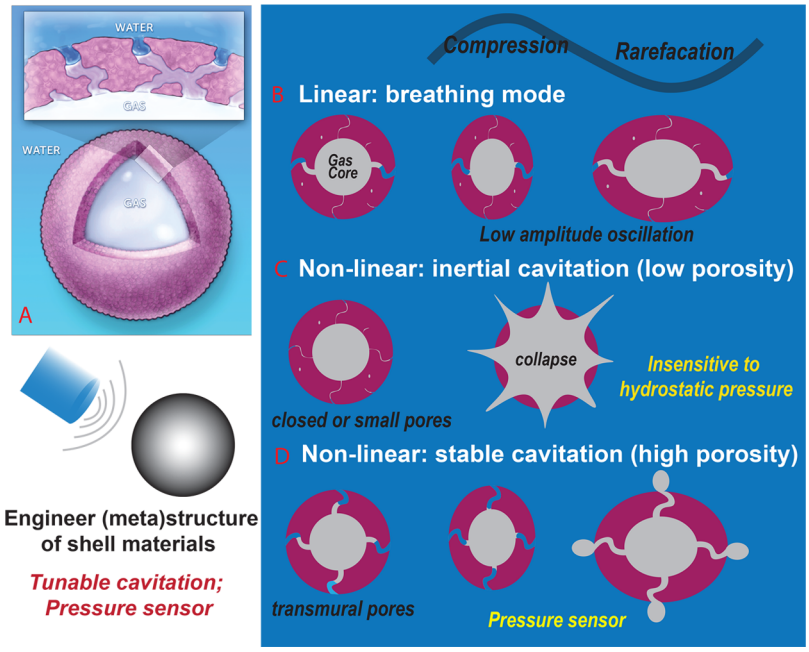

Figure 1. (A) Cartoon illustration of a caged MB that possesses a porous shell consisting of NP aggregates via IFNP. (B–D) Proposed mechanism of the effect of shell metastructure of MBs on their mode of acoustic cavitation. (B) Under low-energy US pulse, both porous and nonporous MBs linearly oscillate in small amplitude, where shell compressibility is the predominate factor. (C) Under high-energy US pulse, for hard-shelled MBs lacking sufficient transmural porosity, any higher-amplitude oscillation is prohibited by the maximal deformability of the shell and is not possible unless inertial cavitation occurs; thus, the shell deformability serves as the main factor to affect nonlinear cavitation of MBs, which is not sensitive to the surrounding pressure. (D) In contrast, for MBs with transmural pores, the open channels in shells provides an extra pathway to dissipate increasing energy from US pulses, thus allowing the MBs to undergo stable cavitation. Because the transmural channels are open, the cavitation of MBs is highly sensitive to hydrostatic pressure.

manipulation alone (e.g., varying output or frequencies) often fails to yield adequate control over the cavitation behaviors of MBs; additionally, available pulse sequences are limited due to a number of practical constraints (e.g, penetration depth, acquisition time, safety considerations). One potential solution to this problem is to develop advanced MB-based materials with tunable acoustic properties that enable the user to tailor the cavitation response to the desired application of interest.

From a materials perspective, the acoustic properties of coated MBs of a given size are largely dictated by the viscoelasticity of the shell.[1] Lipids and proteins are commonly used to stabilize MBs because they form highly elastic (soft) shells and exhibit acoustic behaviors analogous to free bubbles.[1] However, soft-shelled MBs are only transiently stable, as they are prone to outgassing, which causes their shells to buckle, and introduces undesirable alterations in their acoustic response.[11] Soft-shelled MBs also tend to have a short half-life in blood (several minutes) which limits their utility for many in vivo applications.[12] As a result, controlling any type of sustained cavitation response by manipulating pulse conditions alone has remained a challenge. For example, Tao et al.[13] reported that strenuous efforts must be taken to minimize inertial cavitation when trying to maintain stable cavitation of soft-shelled MBs when delivering drugs to the brain. However, such approaches may not be feasible in clinical settings. Hard-shelled polymeric MBs have been developed as a potential alternative, because they are inherently more stable but still permit chemical functionalization and drug loading.[14,15] However, their rigid shells suppress the acoustic response, which has hindered their clinical translation.[16] As the acoustic pressure increases, these hard-shelled MBs more likely undergo unpredictable inertial cavitation, which increases the likelihood of an adverse event.[17]

Despite these obvious shortcomings, little effort has been devoted toward developing material solutions for improving or controlling MB cavitation behavior. As a recent example, the Shapiro group demonstrated the ability to manipulate the internal cavitation threshold by engineering cellular gas vesicles with different shell proteins as a means to enhance US contrast imaging of microorganisms.[18] Synthetic routes that provide similar control over MB acoustic properties would be highly desirable and would greatly expand the clinical utility of US beyond imaging alone. For example, MBs engineered to have high acoustic stability and/or high resonance frequencies (RFs) (e.g., > 10 MHz) may be useful agents to improve contrast-enhanced super-resolution imaging,[19] whereas MBs capable of stable cavitation may be useful for targeted drug delivery or sonoporation. Furthermore, because the MB environment (e.g., pressure, flow, temperature) also influences the cavitation behavior, it should be possible to engineer MB-based acoustic biosensors (i.e., blood pressure).[20,21] Previously, we developed an approach to fabricate stable and porous hard-shelled MBs via interfacial nanoprecipitation (IFNP) of modified dextran polymers.[22,23] Despite low compressibility of their hard shells, some porous MBs unexpectedly yielded robust second harmonic emissions similar to soft-shelled MBs. While our previous work only offered limited tunability to control collapse pressures by varying the shell composition,[22] it suggested that the metastructure (e.g., porosity) of the rigid shells produced by IFNP may provide an untapped opportunity to control acoustic behaviors of MBs. In this report, we show that the IFNP serves as a powerful strategy to fabricate MBs with unprecedented tunability to regulate a full

https://doi.org/10.1021/acsmaterialslett.1c00296
ACS Materials Lett. 2021, 3, 978–987

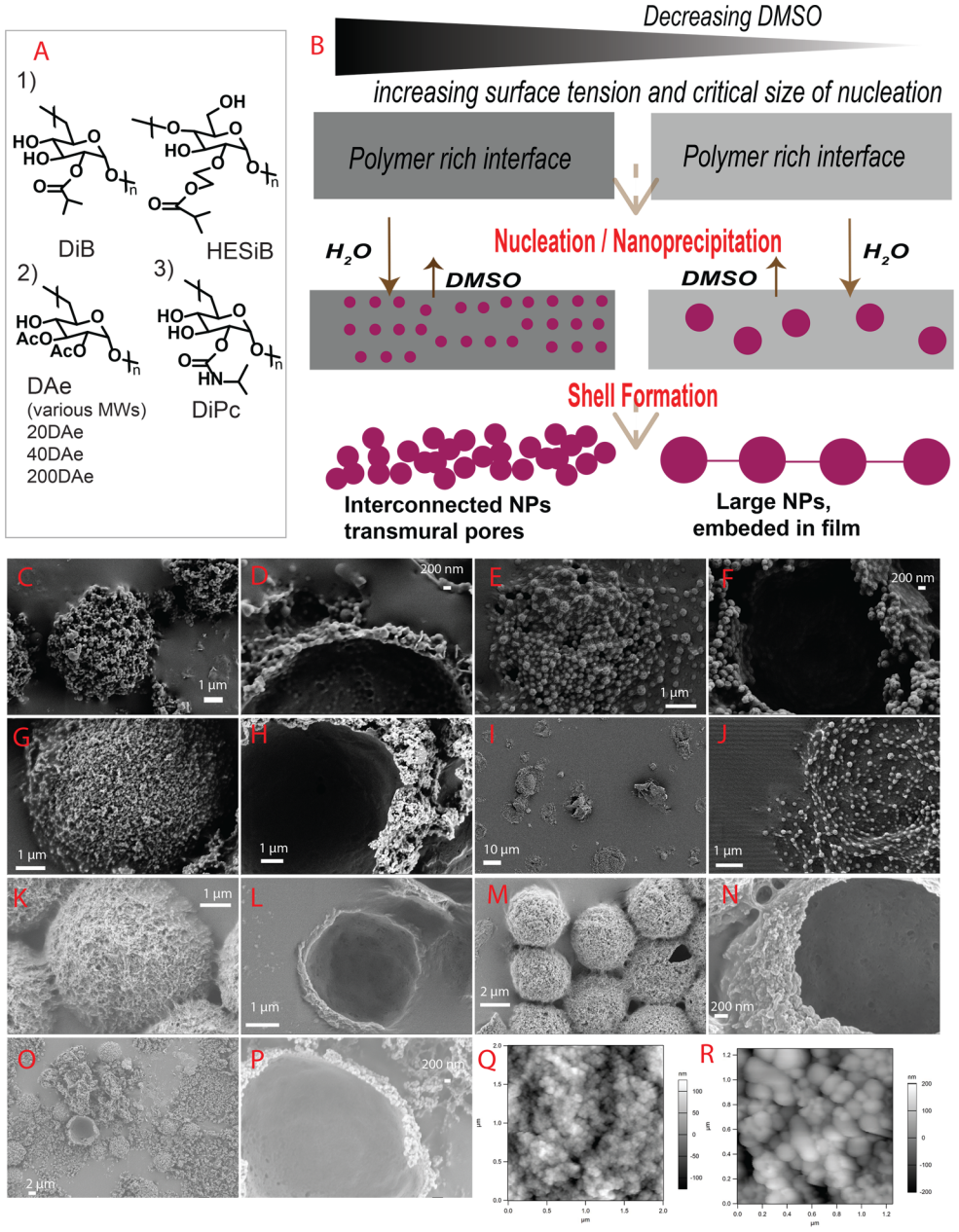

Figure 2. (A) Illustration of the IFNP to form shells of MBs and the effect of solvent. (B) Chemical structures of various modified polymers used in current work. (C−Q) SEM characterization of the surface and cross-section of various MBs; (C,D): DiB (68%), (E,F): DiB (50%), (G,H): HESiB (68%), (I,J): HESiB (50%), (K,L): 20DAe (50%), (M,N): 200DAe (78%), (O,P): DiPc (78%). The percentage in the bracket indicated the DMSO ratio used in MB fabrication. (Q,R): Characterization of surface morphology by AFM of 200DAe (78%) and DiPc (78%) MBs, respectively.

range of their linear and nonlinear cavitation behaviors, and we highlight their potential use and application for, but not limited to, advanced imaging, drug delivery, and pressure sensing applications. We show that these MBs, dubbed "caged MBs" (i.e., a gas core trapped inside a porous shell, Figure 1A), have interesting cavitation features that are attributable to both the shell material properties and their metastructure (e.g., nanoscale porosity, heterogeneity). We believe the lessons accrued from this work offer a different avenue to design acoustic microbubbles for advanced theranostic applications.

MB Design. On the basis of our previous work, we hypothesized that our contrast agents resembled a free microbubble encapsuled within a porous polymeric cage (Figure 1). We suspect that the acoustic response is primarily due to compression and expansion of the free gas bubble within the porous cage that occurs in response to US pulses. Using this model, it follows that the oscillation of the MBs will largely depend on the structure of the porous shell (i.e., void volume, transmural porosity, shell thickness, among others); thus, we hypothesize that the ability to modulate the shell materials (e.g., elasticity) and structure (e.g., porous microstructure) may collectively permit control over acoustic cavitation and generate new acoustic phenomena.

The shell elasticity can be conveniently tuned by modifying the polymeric structures (e.g., varying the functional groups). However, engineering porosity into thin-shelled MBs while preserving the gas core is challenging using conventional methods, particularly transmural porosity, as is required to

https://doi.org/10.1021/acsmaterialslett.1c00296
ACS Materials Lett. 2021, 3, 978−987

increase acoustic responsiveness of solid shelled MBs.[22] We originally introduced the concept of IFNP to fabricate stable pH responsive polymeric MBs for intravenous oxygen delivery;[23] herein, we expanded this method to reveal its utility in tuning the structure of porous shells. Briefly, modified polymers are dissolved into a DMSO (solvent) and H_2O (nonsolvent) mixture and homogenized at the air−liquid (a/l) interface to introduce microbubbles into the system. The polymers behave as surfactants that transiently stabilize the microbubbles by self-assembling at the a/l interface. Upon further dilution with water, the polymers precipitate to form nanoparticle aggregates that assemble at the bubble surface, encapsulating it within a porous polymer shell. In contrast to standard bulk nanoprecipitation,[24,25] the amphiphilicity and solubility of the polymers are manipulated so that nucleation and growth of NPs develop only at the a/l interface.[23] Importantly, similar solvent-induced phase separation strategies have been used for decades to control the porosity of many commercially used polymeric membranes.[26,27] Furthermore, it is well-known that varying the surface tension and solvent type critically influences the morphology of precipitated polymers.[28] Thus, we reasoned that manipulating select key parameters, namely, chemical structure, polymer molecular weight, and solvent parameters, during IFNP would provide a versatile platform to manipulate the evolution of porosity and mechanical properties of the nanoprecipitate shell. To do this, we first synthesized dextran (D) and hydroxyethyl starch (HES) polymers bearing one of three linkages: isobutyryl ester (iB), acetyl ester (Ae), or isopropyl carbamate (iPc). (Figure 2A, for clarity: DiB refers to isobutyryl dextran ester; DAe to acetyl dextran ester, HESiB to isobutyryl hydroxyethyl starch ester; and DiPc to isopropyl dextran carbamate; see SI for details). To illustrate the acoustic−material relationships, and for the purpose of discussion, these polymers have been conceptually divided into three groups (Group 1: DiB and HESiB; Group 2: DAe 20K, 40K, and 200 K, and Group 3: DiPc). Next, these polymers were dissolved into solutions of varying solvent ratio (i.e., DMSO:H2O), homogenized to make air-filled MBs, and their microstructure and mechanical properties analyzed using scanning electron microscopy (SEM) and atomic force microscopy (AFM), respectively (see SI for details). As shown in Figure 2C−J, the effect of solvent ratio on MB shells was most striking for polymers in Group 1 (i.e., DiB and HESiB). Using 68% DMSO, both DiB (68%) and HESiB (68%) MBs were intact after drying and could be resuspended in water, and they possessed thick (100−300 nm) and porous shells with highly irregular surfaces consisting of densely packed aggregates of small NPs (grain size: DiB 100−200 nm, HESiB 30−90 nm). The morphology and tortuosity of the pores were highly reminiscent of those seen in porous membranes at submicron scales created through phase inversion[27,29] (the transmural porosity was further confirmed by surfactant and/or pressurization tests as reported previously,[22] Figure 4S). In contrast, at 50% DMSO, HESiB (50%), and DiB (50%), MBs showed nonporous morphology consisting of large NPs embedded within a thin continuous film (these MBs all collapsed during drying due to a lack of mechanical strength). In Group 2, SEM images of MBs showed that they all had a porous morphology and a shell thickness of several hundred nanometers, and all survived drying and could be resuspended, regardless of the polymer molecular weight (Figure 2K−N, Figures S5, S6). The presence of transmural porosity was further confirmed by surfactant and pressurization tests, both of which led to water influx into the gas core (Figure S8). Unfortunately, we did not observe significant differences in the macroscopic pore morphology, as assessed by SEM; however, varying the MW did reveal an effect on the acoustic properties, as discussed in more detail below. MB shells fabricated from DiPc (Group 3) at 68% DMSO appeared to consist of NP aggregates embedded within a thin polymer film, which collapsed after drying (Figure S7). By increasing the DMSO ratio to 78%, the shell thickness in DiPc MBs increased and became more heterogeneous (Figure 2O,P). The thicker shells appeared to be somewhat porous in SEM images; however, none of the DiPc (78%) MBs resulted in water influx by surfactant nor by pressurization tests (Figure S9), which indicated that DiPc (78%) MBs lack effective transmural porosity. We further analyzed the morphological difference between the transmurally porous 200DAe (78%) and less porous DiPc (78%) MBs using atomic force microscopy (AFM), where the shell of the former revealed much finer porous structures of morphologically more anisotropic growth of NP aggregates similar to typical polymeric nanoporous membranes. We further characterized the polymeric micelles by dynamic light scattering (DLS) in DMSO/water mixture (see detailed discussion in SI). Notably, the micellar size of 200DAe 78% (∼117 nm) was much larger than the grain size of nanoparticles (30−60 nm, Figure 2Q) that formed the final shells, indicating the original micelles were highly swollen and subsequently underwent extensive desolvation which contributes to the porous shells in phase inversion process. Instead, for DiPc 78%, the presence of large grain size (varying from 100 to 200 nm, Figure 2R) of the nanoparticles in MB shells was in more similar range of its micellar size (∼188 nm), and this may suggest their micelles were less swollen and underwent a less-extensive desolvation process, consistent with their lack of porosity. These examples demonstrate the utility of IFNP to engineer stable MBs with diverse shell structures (e.g., from a continuous membrane to a porous cage). We suspect that the underlying mechanism that dictates shell microstructure is an interplay between the polymer structure and the DMSO concentration, which likely influences the evolution of nanoprecipitation via surface tension, viscosity, etc. For instance, conditions that favor lower surface tensions will likely decrease the critical nucleation size, thus increasing the number of nucleation sites and decreasing the growth rate, to yield shells with greater transmural porosity (Figure 2B). The precise mechanism of formation and further manipulations will be elucidated and developed in future studies.

Tuning Linear Acoustic Cavitation. Next, we carried out acoustic studies to investigate how the MB shell structure affected their linear acoustic response to US excitation. We conducted attenuation experiments to study the resonance frequencies (RFs) of our MBs, as this is a common approach for characterizing the acoustic properties of lipid- and polymer-shelled MBs (Figure S10). Attenuation tests were validated by measurement of commercial ultrasound contrast agents that have been characterized previously (Figure S11). The selection of US frequencies for imaging will vary depending on the target tissue; therefore, the ability to modulate the RFs of MBs may maximize their clinical utility of contrast-enhanced imaging. To compare the effects of MB shell structure on RFs, we first obtained near monodispersed MBs (mean size ∼4.5 μm) from Groups 2 and 3 using selective centrifugal separation (Figure

https://doi.org/10.1021/acsmaterialslett.1c00296
ACS Materials Lett. 2021, 3, 978−987

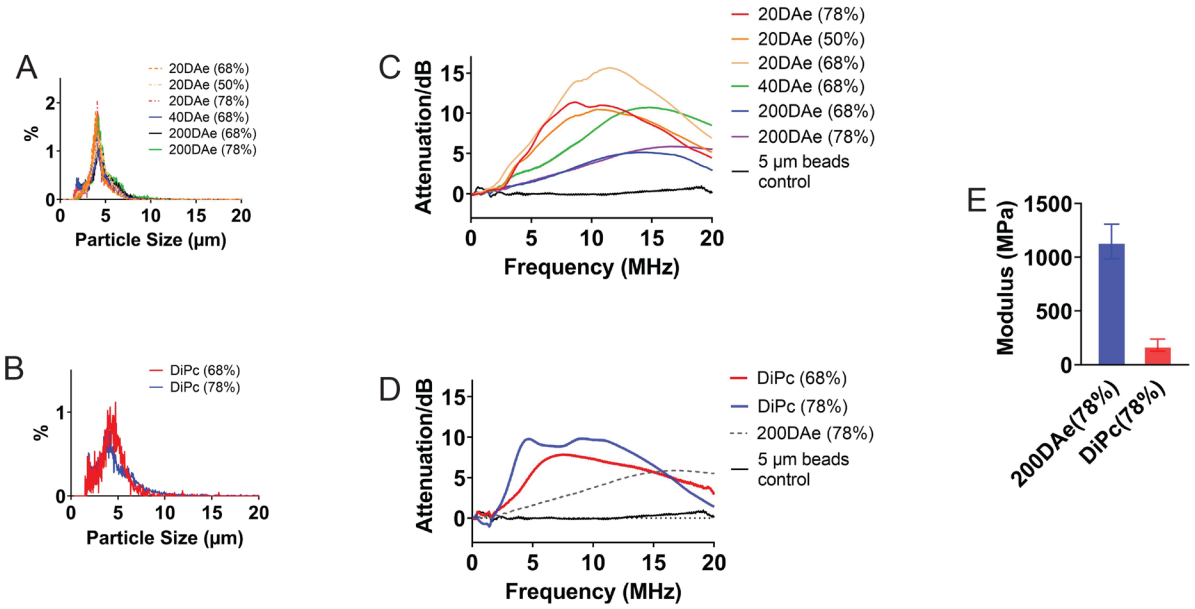

Figure 3. (A,B) Various DAe and DiPc MBs fabricated under different DMSO concentration showed uniform size distribution after centrifugal separation (mean diameter ~ 4.5 μm). (C,D) RFs of DAe and DiPc MBs can be tuned by varying polymer types and MWs, and DMSO concentration during fabrication. (E) AFM measurement of the modulus of 200DAe (78%) and DiPc (78%).

3A,B, SI). In general, the MB RFs could be easily tuned (between 3 and 17 MHz) by varying the MB shell material and shell microstructure. Importantly, this range is well within the US frequencies commonly used for clinical applications. For example, RFs obtained from DAe MBs in Group 2, clearly demonstrated a strong dependence on polymer molecular weight, with higher MWs resulting in higher RFs, likely due to the increased mechanical stiffness (Figure 3C). Further, despite our inability to distinguish an effect of the solvent ratio on the shell microstructure, via SEM, DAe MBs fabricated from different DMSO ratios exhibited varying RFs ranging from 7 to 17 MHz, indicating that the solvent ratio indeed affected finer transmural porosity of the shell and can be used to fine-tune RFs. In comparison, DiPc MBs in Group 3 (Figure 3D), showed much lower RFs, suggesting higher compressibility of the shells compared to DAe MBs.

In principle, the attenuation test provides information on the compressibility of MB shells (Figure 1B), and a higher RF of same sized MBs indicates greater stiffness of the shells.[30] Intrigued by the striking difference in RFs obtained from transmurally porous 200DAe (78%) compared with the less porous DiPc (78%) MBs, we further performed mechanical analysis using AFM on air-dried MBs. The results showed that 200DAe (78%) MBs (modulus: 1146 ± 161 MPa) are about 5 times stiffer than that of DiPc (78%) MBs (modulus: 184 ± 56 MPa, Figure 3E). It is likely that, in comparison with acetyl, the bulkier isopropyl carbamate groups of dextran backbone negatively impacted the stacking of polymeric chains, thus decreasing the elastic modulus. These results were consistent with the trends noted in RF measurements, confirming that the shell compressibility is the predominate factor affecting the RF when MBs undergo small-amplitude linear oscillation. Furthermore, unlike many commercial MBs with sharper RFs that are often below 3 MHz, the RFs of our polymeric MBs display a broad bandwidth, most likely due to the heterogeneity and porosity in shell (meta)structures as observed under SEM. This is advantageous for imaging application because clinical US transducers rely on higher and broadband frequencies. Additionally, our caged MBs with higher RFs (>10 MHz) may be also interesting candidates for super-resolution imaging. Overall, the above results established the robust utility of IFNP to manipulate the linear oscillation of MBs by tuning the polymeric structures and fabrication conditions.

Tuning Nonlinear Acoustic Cavitation. While linear oscillations of MBs at various RFs is the most relevant parameter for general imaging purposes, many advanced applications, such as sonoporation, leverage the nonlinear behavior of MBs when exposed to higher acoustic pressures (in the case of sonoporation this results in bubble cavitation which introduces defects in nearby cell membranes, allowing drugs to enter the cells). To investigate how the shell structure of our caged MBs affect the nonlinear acoustic cavitation, we studied their sub-harmonic emission (SHE), which is a key indicator of nonlinear cavitation.[31,32] SHE plays a critical role in developing safe and effective US therapies and has been utilized to predict the transition of oscillating MBs from stable to inertial cavitation, in which the latter would locally release high heat and violent mechanical energy that may be harmful to healthy tissues. For instance, the ability to minimize inertial cavitation while maintaining stable nonlinear cavitation was critical to ensure safe drug delivery to the brain, while inertial cavitation is often employed for ablation purposes.[13] Furthermore, it was shown recently that the SHE of soft-shelled MBs are sensitive to surrounding environment such as hydrostatic pressure.[33]

To probe the nonlinear behavior of our MBs, we first studied their SHE as a function of acoustic pressure using a low frequency pulse at 0.74 MHz (SI and Figure S12). This frequency was selected because it can be used for both imaging and therapeutic purposes and can penetrate deeper into tissue. As expected, with the increase of acoustic pressure, the SHE increased as coated MBs transitioned from linear to nonlinear oscillations. Interestingly, coated MBs in Groups 2 and 3 exhibited remarkably different SHE profiles, indicating distinct modes of oscillation, with representative 200DAe (78%) and DiPc (78%) MBs shown in Figure 4. Significant SHE in

https://doi.org/10.1021/acsmaterialslett.1c00296
ACS Materials Lett. 2021, 3, 978−987

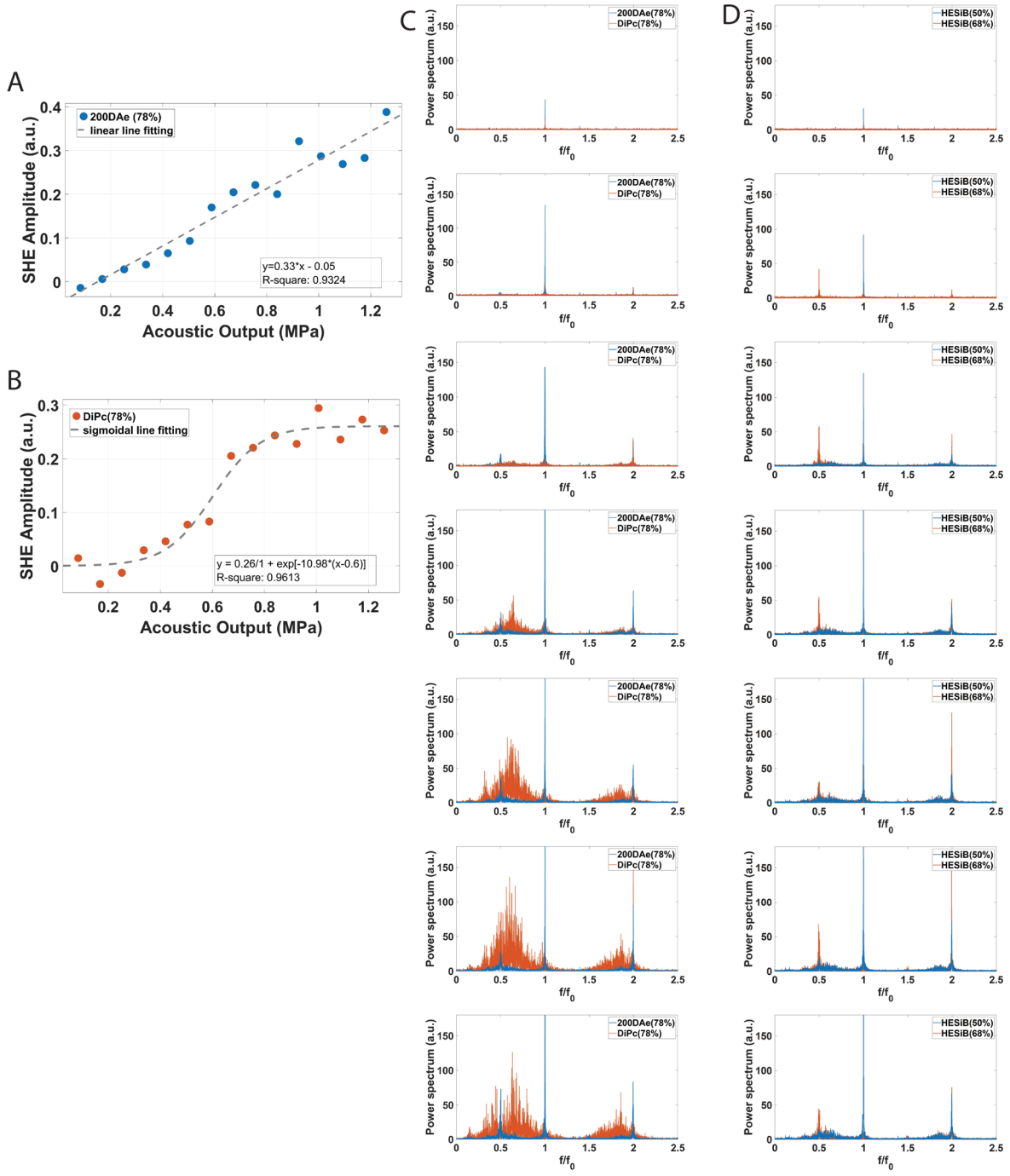

Figure 4. (A) The amplitude of SHE of 200DAe (78%) MBs increased linearly with acoustic output. (B) The SHE of DiPc (78%) MBs increased in response to higher acoustic output and reached a threshold under the current condition. (C) The frequency response curves of 200DAe (78%) and DiPc (78%) MBs under increased acoustic output (from top to bottom: 0.084, 0.252, 0.42, 0.588, 0.756, 0.924, 1.092 MPa), indicating the shell structure regulates the modes of nonlinear cavitation. (D) The frequency response curves of HESiB (50%) and (68%) MBs with increased acoustic output as in C (f_0 = 0.74 MHz).

transmurally porous 200DAe (78%) MBs occurred at 0.42 MPa, as shown by a sharp SHE peak in the frequency curve in response to a relatively low acoustic pressure of 0.42 MPa. The magnitude of SHE increased linearly up to 1.26 MPa (Figure 4A), while maintaining its shape along with a very low level of broadband noise (Figure 4C), suggesting that 200DAe (78%) MBs responded in the mode of stable nonlinear cavitation with tunable amplitude under a wide range of acoustic power. In contrast, the less porous and more elastic DiPc (78%) MBs required higher acoustic energy (>0.5 MPa) to generate detectable SHE emissions (Figure 4B). Moreover, they did not display a distinguishable phase of stable nonlinear cavitation, but transitioned sharply to inertial cavitation with increased acoustic pressure (with a distinct collapse pressure ~0.58 MPa), as indicated by the distortion of SHE peak and extremely high broadband noise in the frequency response curve. These differences in the nonlinear behavior between 200DAe (78%) and DiPc (78%) MBs were striking, and may at first appear to be counterintuitive. For instance, DiPc (78%) MBs possess lower RFs and more compressible shells (as

https://doi.org/10.1021/acsmaterialslett.1c00296
ACS Materials Lett. 2021, 3, 978−987

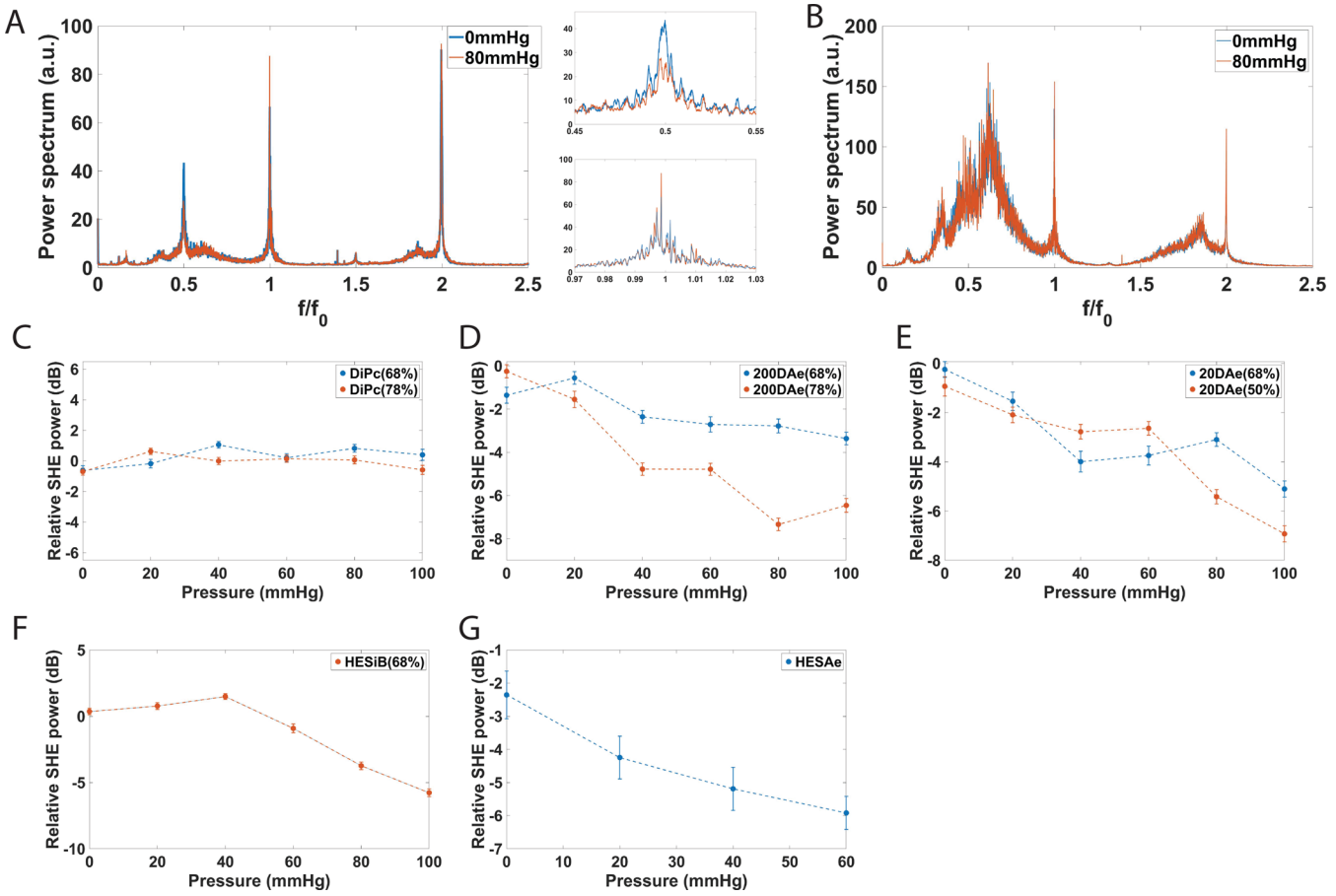

Figure 5. (A) The frequency response curves of 200DAe (78%) MBs showed dependence on hydrostatic pressure. (B) The frequency response curves of DiPc (78%) MBs did not reveal any change upon hydrostatic pressure under the current condition. (C) SHE of various DiPc MBs showed no dependence on hydrostatic pressure (0.8 MPa). (D−G) The SHE of various porous caged MBs exhibited dependence on hydrostatic pressure (D−F: 1 MPa; G: 0.6 MPa), and it showed their sensitivity can be tuned by manipulating shell structures.

shown by AFM results), and therefore, should be more echogenic and expected to exhibit robust stable cavitation. Nonetheless, the observed phenomena can be readily explained with our proposed caged MB model (Figure 1B−D). During RF measurement as in Figure 1B where MBs undergo linear small amplitude oscillation, the carbamate polymeric shells of DiPc (78%) become more deformed than the stiffer 200DAe (78%) shell. However, because DiPc (78%) MBs lack effective transmural porosity in the shell, the maximal amplitude of oscillation is strictly limited by the maximal deformability of the polymeric membrane. Consequently, the DiPc shells effectively prohibit higher amplitude oscillation (stable nonlinear cavitation) by the gas core, unless the shell breaks apart via inertial cavitation (Figure 1B). On the other hand, the porous shell of the stiffer shelled 200DAe (78%) MBs allows the energy of the oscillating gas core to be effectively dissipated through the air−liquid interface within the shell's transmural pores, thus preventing bubble collapse and enabling sustained stable nonlinear cavitation (Figure 1D). Furthermore, to investigate the stability of MBs under physiological condition, we incubated 200DAe (78%) and DiPc (78%) MBs in 50 mg/mL bovine serum albumin (BSA) in PBS buffer to investigate the influence of protein absorption on their acoustic behaviors; this is because serum proteins may absorb on the transmural capillaries thus alter or clog the pores in shells. As shown in SI, both MBs were stable (Figure S13); similar to that in pure water, the SHE of 200DAe in BSA buffer remained following a highly linear trend ($R^2 > 0.95$) indicating stable nonlinear cavitation after 30 min (Figure S14); meanwhile the SHE of DiPc in BSA buffer still fit sigmoidal curves indistinguishable from that in water ($R^2 > 0.95$) (Figure S15). A very slight decrease in SHE of 200DAe in BSA buffer was seen only under high acoustic pressure, this was likely caused by a loss of small MB population that may be caused by BSA absorption onto the outer side of large pores (see more discussion in SI). Nonetheless, these results demonstrated the cavitation mechanisms were not affected by protein absorption under physiological condition. Similar results were also observed for porous HESiB (68%) and nonporous HESiB (50%) MBs, although the slight MB size difference (Figure S16) may slightly complicate the SHE analysis. Regardless, HESiB (68%) MBs possess thicker and more porous shells and exhibited more robust and stable nonlinear cavitation; however, nonporous HESiB (50%) MBs quickly transitioned to inertial cavitation as the acoustic excitation pressure was increased. Together, these results show that caged MBs via IFNP can be designed with well-defined acoustic properties, thus permitting high control over their cavitation behaviors.

SHE-Pressure Sensor. Finally, motivated by both an immediate clinical demand and our basic theoretical understanding of acoustics, we explored the feasibility of using SHE of caged MBs for hydrostatic pressure sensing. At present, the standard approach to monitor intracardiac and intravascular pressure in critical care patients requires catheterization, which

https://doi.org/10.1021/acsmaterialslett.1c00296
ACS Materials Lett. 2021, 3, 978−987

carries considerable risks;[34] hence, developing an accurate noninvasive cardiac pressure sensor using ultrasound will fulfill a significant unmet clinical need. Although SHE of commercially available soft MBs was recently reported to display various types of relationships to hydrostatic pressure (contingent on the shell compositions), their precise mechanisms are unclear,[33,35] and there remain challenges to be addressed, including circulation stability of MBs and data acquisition time.[34] Thus, we conceive the caged MBs with improved control over cavitation are more advantageous to function as pressure sensors. On the basis of our current findings and our working caged MB model, we predicted that transmurally porous MBs may serve as tunable pressure sensors. As shown in Figure 1D, we speculate that the stable nonlinear cavitation of caged MBs mainly depends on the ability to push the air−liquid interface through the transmural channels. We hypothesized that a higher hydrostatic pressure would hinder pulsations of the gas/liquid interface through the open channels and thus decrease the SHE amplitude. To test this hypothesis, we select the acoustic pressure where the SHE of select MBs was reasonably high and broadband noise was minimal (i.e., nonlinear stable cavitation). Then we continuously recorded the SHE of select caged MBs at different hydrostatic pressures in the range of 0 to 100 mmHg (important range for pulmonary artery pressures. Steps were taken to prevent bubble loss; see SI for details). As shown in Figure 5A, the SHE amplitude for transmurally porous 200DAe (78%) MBs had an inverse relationship with hydrostatic pressure but had an increased emission at the linear resonance frequency (f_0); this indicates that stable nonlinear oscillations (Figure 1D) were suppressed by pressurization, while a portion of energy was redistributed back to linear oscillations in breathing mode (Figure 1B). The attenuation of SHE of 200DAe (78%) MBs had a linear relationship to increasing hydrostatic pressure from 0 to 80 mmHg(Figure 5D). In comparison, the frequency response curve of the less porous DiPc (78%) MBs was less sensitive to pressurization under similar conditions (Figure 5B,C), affirming our previous observation that its shell compressibility has a dominant effect on cavitation. The SHE-hydrostatic pressure dependence by various select MBs is shown in Figure 5D−G. To note, the relationship between SHE and hydrostatic pressure varied across polymeric types and shell structures, which likely reflects a finer difference in shell porosity. For example, the 200DAe (78%) MB appeared to have higher pressure sensitivity than 200DAe (75%) MB, likely due to greater transmural porosity in the former when fabricated with higher a DMSO ratio. In contrast, 20DAe MBs fabricated with different DMSO ratio showed a similar pressure sensitivity; these results were not surprising since the high MW 200DAe polymers are less soluble than 20DAe so that its phase separation process is more susceptible to solvent effects. HESiB (68%) MB appeared to be pressure sensitive in the range of 40 to 100 mmHg. Interestingly, replacing the iB group with Ae groups on a HES backbone results in good linear SHE-pressure dependence from 0 to 60 mmHg even with low acoustic output (0.6 MPa). These results demonstrate that IFNP can be utilized to fabricate tunable acoustic pressure biosensors based on our concept of caged MBs with the ability to modulate their pressure sensitivity for clinical applications.

CONCLUSIONS

To conclude, IFNP serves as a useful method to engineer caged MBs with tunable acoustic properties. We show that polymeric materials and shell metastructure (particularly, porosity) together can be manipulated to provide a high level of control over both forced linear and nonlinear oscillations, as well as modulating their sensitivity toward hydrostatic pressures. In contrast to the traditional paradigm of US contrast agent that primarily focus on a model of gas core coated with elastic shells that act as a homogeneous membrane, our current work provides an alternative model of caged MBs with hard nanoporous polymeric shells which possess higher stability and greater tunability to control their cavitation behaviors. This affords new opportunities to design acoustic microbubbles and ultrasound-responsive materials. We expect this approach will readily find applications in advanced imaging, (e.g., supersolution imaging, noninvasive pressure or flow sensing), targeted drug delivery, microsurgery, cancer ablation, tissue engineering, microrobotics, and more.

ASSOCIATED CONTENT

Supporting Information

The Supporting Information is available free of charge at https://pubs.acs.org/doi/10.1021/acsmaterialslett.1c00296.

Materials and general methods, synthesis for polymers, characterizations of polymeric micelles in DMSO/water mixture, additional SEM and optical microscope characterization of MBs, and detailed experimental procedures for acoustic characterizations (PDF)

AUTHOR INFORMATION

Corresponding Authors

Yifeng Peng − *Department of Pediatrics and Department of Cardiology, Boston Children's Hospital, Harvard Medical School, Boston, Massachusetts 02115, United States;* orcid.org/0000-0002-1273-8171; Email: yifeng.peng@childrens.harvard.edu

Brian D. Polizzotti − *Department of Pediatrics and Department of Cardiology, Boston Children's Hospital, Harvard Medical School, Boston, Massachusetts 02115, United States*; Email: brian.polizzotti@gmail.com

Authors

Chenguang Peng − *Department of Radiology, Brigham and Women's Hospital, Boston, Massachusetts 02115, United States; Department of Radiology, Harvard Medical School, Boston, Massachusetts 02115, United States*

Tien Nguyen − *Department of Cardiology, Boston Children's Hospital, Harvard Medical School, Boston, Massachusetts 02115, United States*

Tao Sun − *Department of Radiology, Brigham and Women's Hospital, Boston, Massachusetts 02115, United States; Department of Radiology, Harvard Medical School, Boston, Massachusetts 02115, United States*

Tyrone Porter − *Department of Biomedical Engineering, Cockrell School of Engineering, The University of Texas at Austin, Austin, Texas 78712, United States*

Nathan McDannold − *Department of Radiology, Brigham and Women's Hospital, Boston, Massachusetts 02115, United States; Department of Radiology, Harvard Medical School, Boston, Massachusetts 02115, United States*

John N. Kheir − *Department of Pediatrics and Department of Cardiology, Boston Children's Hospital, Harvard Medical School, Boston, Massachusetts 02115, United States*

Complete contact information is available at: https://pubs.acs.org/10.1021/acsmaterialslett.1c00296

Author Contributions

[¶]Y.P. and C.P. contributed equallyto this work. All authors have given approval to the final version of the manuscript.

Funding

This work was supported by the Office of the Assistant Secretary of Defense for Health Affairs through the Peer Reviewed Medical Research Program under Award Nos. W81XWH-15-1-0544 and W81XWH1910237 (BDP and JNK). Opinions, interpretations, conclusions, and recommendations are those of the author and are not necessarily endorsed by the Department of Defense. Further, it was supported by the National Institute of Heart, Lung, and Blood Institute (1R01HL141818-02, BDP and JNK), a DRIVE grant from the Boston Biomedical Innovation Center (NIH U54HL119145, BDP), President's Innovation Fund and Technology Development Grant from Boston Children's Hospital (BDP and JNK), and the Hess Family Foundation (BDP and JNK). This work is also supported by an OFD Faculty Career Development Fellowship by Boston Children's Hospital (YP), and by an NIH R21EB027506 (TP).

Notes

The authors declare no competing financial interest.

■ ACKNOWLEDGMENTS

The SEM imaging and AFM were performed the Center for Nanoscale Systems (CNS) of Harvard University with assistance by Jason Tresback, which is supported by the National Science Foundation under NSF award no. 1541959. All authors are grateful to Prof. Glynn Holt (Boston University) for his valuable insights that help to improve this work.

■ ABBREVIATIONS

MB	microbubble
US	ultrasound
IFNP	interfacial nanoprecipitation
RF	resonance frequency
SHE	subharmonic emission.

■ REFERENCES

(1) Roovers, S.; Segers, T.; Lajoinie, G.; Deprez, J.; Versluis, M.; De Smedt, S. C.; Lentacker, I. The role of ultrasound-driven microbubble dynamics in drug delivery: from microbubble fundamentals to clinical translation. *Langmuir* **2019**, *35*, 10173−10191.

(2) Frinking, P.; Segers, T.; Luan, Y.; Tranquart, F. Three decades of ultrasound contrast agents: a review of the past, present and future improvements. *Ultrasound Med. Biol.* **2020**, *46*, 892−908.

(3) Lentacker, I.; De Cock, I.; Deckers, R.; De Smedt, S. C.; Moonen, C. T. W. Understanding ultrasound induced sonoporation: definitions and underlying mechanisms. *Adv. Drug Delivery Rev.* **2014**, *72*, 49−64.

(4) Chowdhury, S. M.; Abou-Elkacem, L.; Lee, T.; Dahl, J.; Lutz, A. M. *J. Controlled Release* **2020**, *326*, 75−90.

(5) Zhou, Y.; Wang, Z.; Chen, Y.; Shen, H.; Luo, Z.; Li, A.; Wang, Q.; Ran, H.; Li, P.; Song, W.; Yang, Z.; Chen, H.; Wang, Z.; Lu, G.; Zheng, Y.; et al. Microbubbles from gas-generating perfluorohexane nanoemulsions for targeted temperature-sensitive ultrasonography and synergistic HIFU ablation of tumors. *Adv. Mater.* **2013**, *25*, 4123−4130.

(6) Errico, C.; Pierre, J.; Pezet, S.; Desailly, Y.; Lenkei, Z.; Couture, O.; Tanter, M. Ultrafast ultrasound localization microscopy for deep super-resolution vascular imaging. *Nature* **2015**, *527*, 499−502.

(7) Hudson, J. M.; Karshafian, R.; Burns, P. N. Quantification of flow using ultrasound and microbubbles: a disruption replenishment model based on physical principles. *Ultrasound Med. Biol.* **2009**, *35*, 2007−2020.

(8) Lu, Y.; Wang, J.; Huang, R.; Chen, G.; Zhong, L.; Shen, S.; et al. Microbubble-mediated sonothrombolysis improves outcome after thrombotic microembolism-induced acute ischemic stroke. *Stroke* **2016**, *47*, 1344−1353.

(9) Ren, L.; Nama, N.; McNeill, J. M.; Soto, F.; Yan, Z.; Liu, W.; Wang, W.; Wang, J.; Mallouk, T. E. 3D steerable, acoustically powered microswimmers for single-particle manipulation. *Sci. adv* **2019**, *5*, No. eaax3084.

(10) Marmottant, P.; Bouakaz, A.; de Jong, N.; Quilliet, C. Buckling resistance of solid shell bubbles under ultrasound. *J. Acoust. Soc. Am.* **2011**, *129*, 1231−1239.

(11) Garg, S.; Thomas, A. A.; Borden, M. A. The effect of lipid monolayer in-plane rigidity on in vivo microbubble circulation persistence. *Biomaterials* **2013**, *34*, 6862−6870.

(12) Narayan, P.; Wheatley, M. A. Preparation and characterization of hollow microcapsules for use as ultrasound contrast agents. *Polym. Eng. Sci.* **1999**, *39*, 2242−2255.

(13) Sun, T.; Zhang, Y.; Power, C.; Alexander, P. M.; Sutton, J. T.; Aryal, M.; Vykhodtseva, N.; Miller, E. L.; McDannold, N. J. Closed-loop control of targeted ultrasound drug delivery across the blood-brain/tumor barriers in a rat glioma model. *Proc. Natl. Acad. Sci. U. S. A.* **2017**, *114*, E10281−E10290.

(14) Song, R.; Peng, C.; Xu, X.; Wang, J.; Yu, M.; Hou, Y.; Zou, R.; Yao, S. Controllable formation of monodisperse polymer microbubbles as ultrasound contrast agents. *ACS Appl. Mater. Interfaces* **2018**, *10*, 14312−14320.

(15) Domenici, F.; Brasili, F.; Oddo, L.; Cerroni, B.; Bedini, A.; Bordi, F.; Paradossi, G. Long-term physical evolution of an elastomeric ultrasound contrast microbubble. *J. Colloid Interface Sci.* **2019**, *540*, 185−196.

(16) Paefgen, V.; Doleschel, D.; Kiessling, F. Evolution of contrast agents for ultrasound imaging and ultrasound-mediated drug delivery. *Front. Pharmacol.* **2015**, *6*, 197.

(17) Izadifar, Z.; Babyn, P.; Chapman, D. Mechanical and biological effects of ultrasound: a review of present knowledge. *Ultrasound Med. Biol.* **2017**, *43*, 1085−1104.

(18) Lakshmanan, A.; Farhadi, A.; Nety, S. P.; Lee-Gosselin, A.; Bourdeau, R. W.; Maresca, D.; Shapiro, M. G. Molecular engineering of acoustic protein nanostructures. *ACS Nano* **2016**, *10*, 7314−7322.

(19) Christensen-Jeffries, K.; Couture, O.; Dayton, P. A.; Eldar, Y. C.; Hynynen, K.; Kiessling, F.; et al. Super-resolution ultrasound imaging. *Ultrasound Med. Biol.* **2020**, *46*, 865−891.

(20) Walker, J. A.; Wang, X.; Peter, K.; Kempe, K.; Corrie, S. R. Dynamic solid-state ultrasound contrast agent for monitoring pH fluctuations in vivo. *ACS Sens* **2020**, *5*, 1190−1197.

(21) Leow, C. H.; Iori, F.; Corbett, R.; Duncan, N.; Caro, C.; Vincent, P.; Tang, M.-X. Microbubble Void Imaging: A Non-invasive Technique for Flow Visualisation and Quantification of Mixing in Large Vessels Using Plane Wave Ultrasound and Controlled Microbubble Contrast Agent Destruction. *Ultrasound Med. Biol.* **2015**, *41*, 2926−2937.

(22) Peng, Y.; Li, Q.; Seekell, R. R.; Kheir, J. N.; Porter, T. M.; Polizzotti, B. D. Tunable nonlinear acoustic reporters using micro- and nanosized air bubbles with porous polymeric hard shells. *ACS Appl. Mater. Interfaces* **2019**, *11*, 7−12.

(23) Peng, Y.; Seekell, R. P.; Cole, A. R.; Lamothe, J. R.; Lock, A. T.; van den Bosch, S.; Tang, X.; Kheir, J. N.; Polizzotti, B. D. Interfacial nanoprecipitation toward stable and responsive microbubbles and their use as a resuscitative fluid. *Angew. Chem., Int. Ed.* **2018**, *57*, 1271−1276.

(24) Schubert, S.; Delaney, J. T., Jr.; Schubert, U. S. Nanoprecipitation and nanoformulation of polymers: from history to powerful possibilities beyond poly(lactic acid). *Soft Matter* **2011**, *7*, 1581−1588.
(25) Lepeltier, E.; Bourgaux, C.; Couvreur, P. Nanoprecipitation and the "ouzo effect": application to drug delivery devices. *Adv. Drug Delivery Rev.* **2014**, *71*, 86−97.
(26) Hołda, A. K.; Vankelecom, I. F.J. Understanding and guiding the phase inversion process for synthesis of solvent resistant nanofiltration membranes. *J. Appl. Polym. Sci.* **2015**, *132*, 42130.
(27) Heo, J.; Choi, Y.; Chung, K. Y.; Park, J. H. Controlled pore evolution during phase inversion from the combinatorial non-solvent approach: application to battery separators. *J. Mater. Chem. A* **2016**, *4*, 9496−9501.
(28) Thanh, N. T. K.; Maclean, N.; Mahiddine, S. Mechanisms of nucleation and growth of nanoparticles in solution. *Chem. Rev.* **2014**, *114*, 7610−7630.
(29) Koromilas, N. D.; Anastasopoulos, C.; Oikonomou, E. K.; Kallitsis, J. K. Preparation of porous polymeric membranes based on a pyridine containing aromatic polyether sulfone. *Polymers* **2019**, *11*, 59.
(30) Versluis, M.; Stride, E.; Lajoinie, G.; Dollet, B.; Segers, T. Ultrasound contrast agent modeling: a review. *Ultrasound Med. Biol.* **2020**, *46*, 2117−2144.
(31) Bader, K. D.; Holland, C. K. Gauging the likelihood of stable cavitation from ultrasound contrast agents. *Phys. Med. Biol.* **2013**, *58*, 127−144.
(32) Sijl, J.; Dollet, B.; Overvelde, M. L. J.; Garbin, V.; Rozendal, T.; de Jong, N.; Lohse, D.; Versluis, M. Subharmonic behavior of phospholipid-coated ultrasound contrast agent microbubbles. *J. Acoust. Soc. Am.* **2010**, *128*, 3239−3252.
(33) Gupta, I.; Eisenbrey, J. R.; Machado, P.; Stanczak, M.; Wallace, K.; Forsberg, F. On factor affecting subharmonic-aided pressure estimation. *Ultrason. Imaging* **2019**, *41*, 35−48.
(34) Dave, J. K.; Kulkarni, S. V.; Pangaonkar, P. P.; Stanczak, M.; McDonald, M. E.; Cohen, I. S.; Mehrotra, P.; Savage, M. P.; Walinsky, P.; Ruggiero, N. J.; Fischman, D. L.; Ogilby, D.; VanWhy, C.; Lombardi, M.; Forsberg, F.; et al. Non-invasive intra-cardiac pressure measurements using subharmonic-acided pressure estimation: proof of concept in humans. *Ultrasound Med. Biol.* **2017**, *43*, 2718−2724.
(35) Nio, A. Q. X.; Faraci, A.; Christensen-Jeffries, K.; Raymond, J. L.; Monaghan, M. J.; Fuster, D.; Forsberg, F.; Eckersley, R. J.; Lamata, P. Optimal control of SonoVue microbubbles to estimate hydrostatic pressure. *IEEE Trans. Ultrason. Ferroelectr. Frq. Control.* **2020**, *67*, 557−567.

https://doi.org/10.1021/acsmaterialslett.1c00296
ACS Materials Lett. 2021, 3, 978−987